Modelling of MIMO Vehicle-to-Vehicle Fading Channels in T-Junction Scattering Environments

He Zhiyi [#1], Chen Wei [#], Zhou Wei [#], Matthias Pätzold [*], Ali Chelli [*]

[#] *School of Information Engineering, WuHan University of Technology*
WuHan, 430070, HuBei, P.R. China
[1] e-mail: hezhiyi@whut.edu.cn

[*] *Faculty of Science and Engineering, University of Agder*
P.O. Box 509, 4898 Grimstad, Norway

***Abstract*— In this paper, a new wideband multiple-input multiple-output (MIMO) fading channel model for vehicle-to-vehicle (V2V) communications is proposed. The MIMO V2V channel model, called for brevity T-model, captures the propagation effects that occur if vehicles move towards a junction with a side road and corner buildings. The starting point for the derivation of the T-model is a new geometric T-junction scattering model, where both single- and double-bounce scattering mechanisms are assumed. Our geometry-based channel model takes into account the exact relationship between the angle-of-arrival (AOA) and the angle-of-departure (AOD). The statistical properties of the T-model are studied under the assumption of non-isotropic scattering. An analytical solution is provided for the space-time-frequency cross-correlation function (STF-CCF) from which several other important characteristic quantities like the temporal autocorrelation function (ACF) can directly be obtained. The achieved theoretical results are illustrated for a typical T-junction propagation scenario. This research work provides designers of MIMO V2V communication systems an important tool in form of a wideband spatial channel model enabling the performance analysis of new high data rate transmission schemes under propagation conditions occurring at T-junctions.**

I. Introduction

Vehicle-to-vehicle (V2V) communication systems are an emerging technology, which is expected to play an important role in ad hoc networks and intelligent transportation systems. This fact has motivated standardization bodies and research institutes to establish a standard for V2V communications, called dedicated short range communication (DSRC) [1]. To develop future V2V communication systems, an exact knowledge of the underlying fading channel is of crucial importance. Since the statistical properties of V2V mobile radio channels differ considerably from the propagation characteristics in present day cellular mobile communication systems, new channel models for V2V communications are needed.

In this context—starting from the well-known geometric two-ring scattering model—a reference model and a simulation model for MIMO V2V channels have been derived in [2]. In [3], a ray-optical approach has been applied to model the wave propagation in inter-vehicle communication environments. Recent work in [4] has gathered measurement data for V2V MIMO radio channels at 5.2 GHz. In addition, the statistical properties of the channel, including the pathloss, the power delay profile, and the delay Doppler spectra have been investigated.

Geometry-based channel models, such as the one-ring model [5], [6], the two-ring model [2], [7], and the elliptical model [8] constitute an important category of channel models. Unfortunately, these geometric channel models cannot be utilized to describe accurately the propagation conditions of V2V channels along streets. Therefore, a special geometric street model has been introduced in [9]. In fact, it has been stated in [10] that the wave propagation along streets can be described by specific geometry-based channel models, where the scatterers are located on straight lines. The street model proposed in [9] can be used for straight streets, but not for street intersections. For such scenarios, a new geometry-based channel model was proposed in [11].

In this paper, a wideband MIMO V2V channel model is derived from a geometric T-junction scattering model. Wideband MIMO V2V channel models constitute the basis for the development of high data rate V2V communication systems. The geometric T-model is used for modelling the scattering environment in case of a street intersection. A typical propagation environment for a street intersection is shown in Fig. 1, in which the transmitter and the receiver are moving towards an intersection point. The propagation environment contains several fixed scatterers located on both sides of the street. The geometric T-model allows the establishment of the exact relationship between the angle-of-arrival (AOA) and angle-of-departure (AOD). This relationship is important for the derivation of the stochastic T-model. Furthermore, we take into account the contribution of single-bounce and double-bounce scattering mechanism. Measurement results in [12] showed that both double-bounce and single-bounce scattering should be considered for V2V channels. Moreover, the statistical properties of the T-model are studied. Analytical solutions are provided for the space-time-frequency cross-correlation function (STF-CCF).

The remainder of this paper is outlined as follows. Section II describes the underlying geometric T-junction scattering model. Starting from this geometric T-model, we present

the corresponding stochastic wideband MIMO V2V channel model in Section III. Its statistical properties are analysed in Section IV. Section V presents some numerical results. Finally, the conclusions are drawn in Section VI.

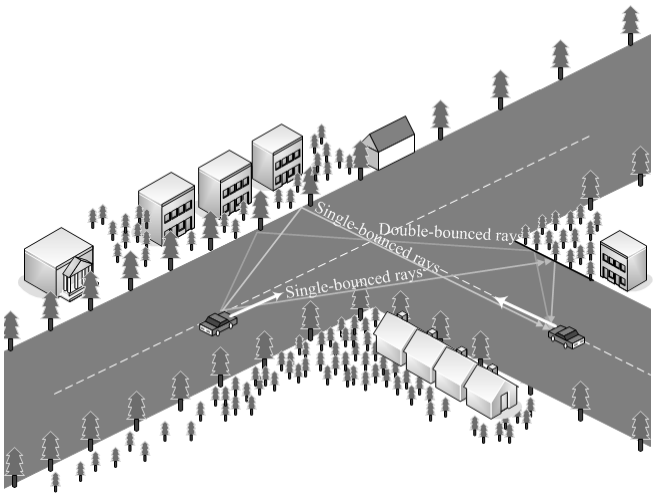

Fig. 1. Typical propagation scenario at a T-junction.

II. The Geometric T-Junction Scattering Model

The statistical properties of the fading channel depend strongly on the location of the scatterers around the transmitter and the receiver. For the design of Euclidean-geometry-based channel models it is a crucial task to find a realistic geometric scattering model that appropriately describes the propagation environment under study.

For the T-junction propagation environment, we propose the geometric scattering model shown in Fig. 2. This geometric T-junction scattering model is the starting point for the derivation of a new stochastic MIMO V2V channel model. As shown in Fig. 2, the transmitter and the receiver are respectively heading with the mobile speeds v_T and v_R towards a T-junction. The transmitter and the receiver are equipped with low-elevation linear antenna arrays consisting of M_T and M_R antenna elements, respectively. The scatterers close the transmitter are denoted by S_m^T $(m = 1, 2, \ldots, M)$, while the symbol S_n^R $(n = 1, 2, \ldots, N)$ designates the scatterers nearby the receiver. The transmitter (receiver) is located at a distance h_1^T (h_1^R) from the left-hand side of the street and at a distance h_2^T (h_2^R) from the right-hand side. At the transmitter side, the AODs are described by the symbols α_m^T and α_n^R. Analogously, at the receiver side, the AODs are denoted by β_m^T and β_n^R. The antenna element spacings at the transmitter and the receiver antenna array are denoted by δ_T and δ_R, respectively. Since the antenna element spacings are small in comparison to $\min\{h_1^T, h_2^T\}$ and $\min\{h_1^R, h_2^R\}$, it is reasonable to assume that the inequalities $(M_T - 1)\delta_T \ll \min\{h_1^T, h_2^T\}$ and $(M_R - 1)\delta_R \ll \min\{h_1^R, h_2^R\}$ hold. It is furthermore assumed that the wave propagation takes place in the two-dimensional plane under non-line-of-sight conditions.

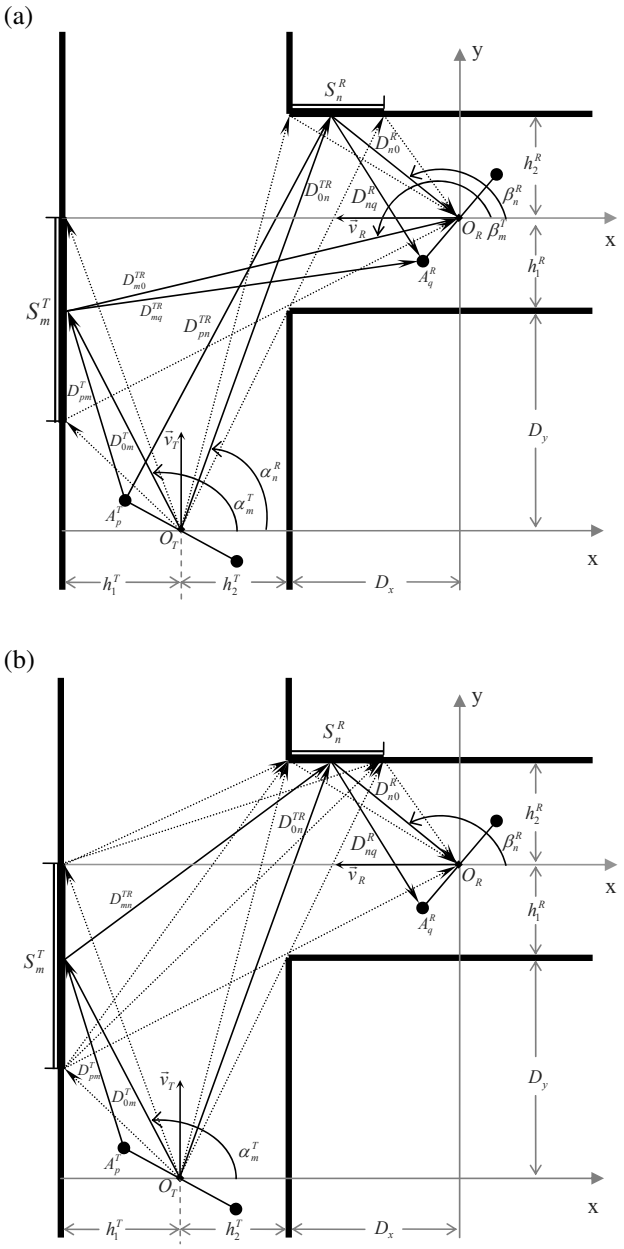

Fig. 2. The geometric T-junction scattering model illustrating (a) the single-bounce and (b) the double-bounce scattering mechanism.

III. The Stochastic MIMO V2V Channel Model

The geometric T-junction scattering model presented in Fig. 2 describes the scattering environment of the channel. It constitutes the starting point for the derivation of a new stochastic wideband MIMO V2V channel model, which is called henceforth the (stochastic) T-model. The temporal, spatial, and frequency characteristics of the T-model are completely determined by the $M_R \times M_T$ channel matrix $\boldsymbol{H}(f', t) = [H_{pq}(f', t)]_{M_R \times M_T}$, where $H_{pq}(f', t)$ denotes the time-variant transfer function of the channel describing the link from the pth element A_p^T of the transmitting antenna to the qth element A_q^R of the receiving antenna. The time-

variant transfer function $H_{pq}(f',t)$ of the link A_p^T–A_q^R can be expressed as a superposition of single-bounce and double-bounce components as follows

$$H_{pq}(f',t) = H_{pq}^{\mathrm{SBT}}(f',t) + H_{pq}^{\mathrm{SBR}}(f',t) + H_{pq}^{\mathrm{DB}}(f',t). \quad (1)$$

Applying the design techniques described in detail in [2] on the geometric T-junction scattering model shown in Fig. 2, results in the following expression for the single- and double-bounce components of the time-variant transfer function:

$$\begin{aligned} H_{pq}^{\mathrm{SBT}}(f',t) &= \lim_{M\to\infty} \sqrt{\frac{\eta_{\mathrm{SBT}}}{M}} \sum_{m=1}^{M} d_m^T\, a_m^T\, b_m^T \\ &\quad \cdot e^{\,j[\theta_m + (f_m^T + f_m^R)t - 2\pi f' \tau'_{pmq}]} \quad (2) \\ H_{pq}^{\mathrm{SBR}}(f',t) &= \lim_{N\to\infty} \sqrt{\frac{\eta_{\mathrm{SBR}}}{N}} \sum_{n=1}^{N} d_n^R\, a_n^R\, b_n^R \\ &\quad \cdot e^{\,j[\theta_n + (f_n^T + f_n^R)t - 2\pi f' \tau'_{pnq}]} \quad (3) \\ H_{pq}^{\mathrm{DB}}(f',t) &= \lim_{M,N\to\infty} \sqrt{\frac{\eta_{\mathrm{DB}}}{MN}} \sum_{m=1}^{M}\sum_{n=1}^{N} d_{mn}^{TR}\, a_m^T\, b_n^R \\ &\quad \cdot e^{\,j[\theta_{mn} + (f_m^T + f_n^R)t - 2\pi f' \tau'_{pmnq}]} \quad (4) \end{aligned}$$

where

$$\begin{aligned} d_m^T &= e^{\,j\frac{2\pi}{\lambda}\left(\frac{h_1^T}{\cos(\alpha_m^T)} + \frac{h_1^T + h_2^T + D_x}{\cos(\beta_m^T)}\right)} \quad (5) \\ d_n^R &= e^{\,-j\frac{2\pi}{\lambda}\left(\frac{D_y + h_1^R + h_2^R}{\sin(\alpha_n^R)} + \frac{h_2^R}{\sin(\beta_n^R)}\right)} \quad (6) \\ d_{mn}^{TR} &= e^{\,-j\frac{2\pi}{\lambda}\left(\frac{h_1^T}{\cos(\alpha_m^T)} + \frac{h_2^R}{\sin(\beta_n^R)} D_{mn}^{TR}\right)} \quad (7) \\ a_m^T &= e^{\,j\frac{2\pi}{\lambda}(M_T - 2p + 1)\frac{\delta_T}{2}\cos(\alpha_m^T - \gamma_T)} \quad (8) \\ a_n^R &= e^{\,j\frac{2\pi}{\lambda}(M_T - 2p + 1)\frac{\delta_T}{2}\cos(\alpha_n^R - \gamma_T)} \quad (9) \\ b_m^T &= e^{\,j\frac{2\pi}{\lambda}(M_R - 2q + 1)\frac{\delta_R}{2}\cos(\beta_m^T - \gamma_R)} \quad (10) \\ b_n^R &= e^{\,j\frac{2\pi}{\lambda}(M_R - 2q + 1)\frac{\delta_R}{2}\cos(\beta_n^R - \gamma_R)} \quad (11) \\ f_m^T &= 2\pi f_{\max}^T t \cos(\phi_T - \alpha_m^T) \quad (12) \\ f_n^T &= 2\pi f_{\max}^T t \cos(\phi_T - \alpha_n^R) \quad (13) \\ f_m^R &= 2\pi f_{\max}^R t \cos(\phi_R - \beta_m^T) \quad (14) \\ f_n^R &= 2\pi f_{\max}^R t \cos(\phi_R - \beta_n^R) \quad (15) \end{aligned}$$

and

$$\begin{aligned} D_{mn}^{TR} &= \big\{[D_x + h_1^T + h_2^T + h_2^R\cot(\beta_n^R)]^2 \\ &\quad + [D_y + h_1^R + h_2^R + h_1^T\tan(\alpha_m^T)]^2\big\}^{1/2}. \quad (16) \end{aligned}$$

In the equations above, the parameters η_{SBT}, η_{SBR}, and η_{DB} define the mean power of the single- and double-bounce components. On these quantities, we impose the boundary condition $\eta_{\mathrm{SBT}} + \eta_{\mathrm{SBR}} + \eta_{\mathrm{DB}} = 1$ to ensure that the average power of the overall stochastic T-model is normalized to unity. The phases θ_m, θ_n, and θ_{mn} are independent identically distributed random variables, each having a uniform distribution over the interval from 0 to 2π. The quantities α_m^T and α_n^R are the AODs, and β_m^T and β_n^R denote the AOAs, as illustrated in Fig. 2. Furthermore, γ_T and γ_R indicate the antenna tilt angles w.r.t. the x-axis at the transmitter and the receiver, respectively. The symbols $f_{\max}^T$ and $f_{\max}^R$ are referred to as the maximum Doppler frequency associated with the mobility of the transmitter and the receiver, respectively. Finally, λ denotes the wavelength.

The propagation delays τ'_{pmq} in (2) are determined by $\tau'_{pmq} = D_{pmq}/c_0$, where c_0 denotes the speed of light and D_{pmq} is the length of the path from the antenna element A_p^T to the antenna element A_q^R via the scatterer S_m^T. With the help of Fig. 2(a), we can expressed the path length D_{pmq} as

$$D_{pmq} = D_{pm}^T + D_{mq}^{TR} \quad (17)$$

where

$$\begin{aligned} D_{pm}^T &= D_{0m}^T - (M_T - 2p + 1)\frac{\delta_T}{2}\cos(\alpha_m^T - \gamma_T) \quad (18) \\ D_{mq}^{TR} &= D_{m0}^{TR} - (M_R - 2q + 1)\frac{\delta_R}{2}\cos(\beta_m^T - \gamma_R) \quad (19) \end{aligned}$$

with $D_{0m}^T = -h_1^T/\cos(\alpha_m^T)$ and $D_{m0}^{TR} = -(D_x + h_1^T + h_2^T)/\cos(\beta_m^T)$.

Analogously, the propagation delays τ'_{pnq} in (3) are given by $\tau'_{pnq} = D_{pnq}/c_0$, where D_{pnq} denotes the length of the path from the antenna element A_p^T to the antenna element A_q^R via the scatterer S_n^R. The path length D_{pnq} can be written as

$$D_{pnq} = D_{pn}^{TR} + D_{nq}^R \quad (20)$$

where

$$\begin{aligned} D_{pn}^{TR} &= D_{0n}^{TR} - (M_T - 2p + 1)\frac{\delta_T}{2}\cos(\alpha_n^R - \gamma_T) \quad (21) \\ D_{nq}^R &= D_{n0}^R - (M_R - 2q + 1)\frac{\delta_R}{2}\cos(\beta_n^R - \gamma_R) \quad (22) \end{aligned}$$

with $D_{0n}^{TR} = (D_y + h_1^R + h_2^R)/\sin(\alpha_n^R)$ and $D_{n0}^R = h_2^R/\sin(\beta_n^R)$.

Finally, the propagation delays τ'_{pmnq} of the double-bounce component [see (4)] are determined by $\tau'_{pmnq} = D_{pmnq}/c_0$, where D_{pmnq} denotes the length of the overall path from the antenna element A_p^T to the antenna element A_q^R via the scatterers S_m^T and S_n^R. With reference to Fig. 2(b), the path length D_{pmnq} can be expressed as

$$D_{pmnq} = D_{pm}^T + D_{mn}^{TR} + D_{nq}^R \quad (23)$$

where D_{pm}^T, D_{mn}^{TR}, and D_{nq}^R are given by (18), (16), and (22), respectively.

We note that for the single-bounce component, the AOA β_m^T (β_n^R) is dependent on the AOD α_m^T (α_n^R). The exact relationships between the AOAs and the AODs can be deduced from Fig. 2. The final results are presented in the appendix.

IV. The Statistical Properties of the T-Model

In this section, we present the STF-CCF of the MIMO V2V channel model and show how other important correlation functions can be derived therefrom.

The STF-CCF is defined as

$$r_{pq,p'q'}(\delta_T, \delta_R, \upsilon', \tau) := E\{H_{pq}(f',t)^* H_{p'q'}(f' + \upsilon', t + \tau)\} \quad (24)$$

where $p, p' \in \{1, 2, \ldots, M_T\}$ and $q, q' \in \{1, 2, \ldots, M_R\}$. Substituting (1) in (24) and applying the techniques described in [2], allows us to express the STF-CCF in the limits $M, N \to \infty$ by the following expression

$$
\begin{aligned}
&r_{pq,p'q'}(\delta_T, \delta_R, \upsilon', \tau) = \\
&\quad \eta_{\mathrm{SBT}} \int_{\alpha^T_{min}}^{\alpha^T_{\max}} g^T \, e^{\,j[(f^T_m + f^R_m)\tau - 2\pi\upsilon'\tau'_{pmq}]} \, p_{\alpha^T}(\alpha^T) \, d\alpha^T \\
&\quad + \eta_{\mathrm{SBR}} \int_{\alpha^R_{\min}}^{\alpha^R_{\max}} g^R e^{\,j[(f^T_n + f^R_n)\tau - 2\pi\upsilon'\tau'_{pnq}]} \, p_{\alpha^R}(\alpha^R) \, d\alpha^R \\
&\quad + \eta_{\mathrm{DB}} \int_{\alpha^T_{\min}}^{\alpha^T_{\max}} \int_{\beta^R_{\min}}^{\beta^R_{\max}} g^{TR} \, e^{\,j[(f^T_m + f^R_n)\tau - 2\pi\upsilon'\tau'_{pmnq}]} \\
&\quad \cdot p_{\alpha^T}(\alpha^T) \, p_{\beta^R}(\beta^R) \, d\beta^R \, d\alpha^T
\end{aligned} \tag{25}
$$

where the upper and lower limits of the integrals are presented in the appendix, and

$$g^T = e^{\,j\frac{2\pi}{\lambda}[(p-p')\delta_T \cos(\alpha^T - \gamma_T) + (q-q')\delta_R \cos(\beta^T - \gamma_R)]} \tag{26}$$

$$g^R = e^{\,j\frac{2\pi}{\lambda}[(p-p')\delta_T \cos(\alpha^R - \gamma_T) + (q-q')\delta_R \cos(\beta^R - \gamma_R)]} \tag{27}$$

$$g^{TR} = e^{\,j\frac{2\pi}{\lambda}[(p-p')\delta_T \cos(\alpha^T - \gamma_T) + (q-q')\delta_R \cos(\beta^R - \gamma_R)]}. \tag{28}$$

We note that as the number of scatterers M and N tends to infinity, the discrete-type random variables α^T_m, α^R_n, and β^R_n become continuous-type random variables (α^T, α^R, and β^R), which are characterized by the probability density functions $p_{\alpha^T}(\alpha^T), p_{\alpha^R}(\alpha^R)$, and $p_{\beta^R}(\beta^R)$, respectively.

The spatial CCF $\rho_{pq,p'q'}(\delta_T, \delta_R)$ is defined as $\rho_{pq,p'q'}(\delta_T, \delta_R) := E\{H_{pq}(f', t)^* H_{p'q'}(f', t)\}$. This function can be obtained from the STF-CCF in (25) by setting $\upsilon' = 0$ and $\tau = 0$, i.e., $\rho_{pq,p'q'}(\delta_T, \delta_R) = r_{pq,pq}(\delta_T, \delta_R, 0, 0)$.

The temporal ACF $r_{pq}(\tau)$ is defined as $r_{pq}(\tau) := E\{H_{pq}(t)^* H_{pq}(t+\tau)\}$ and can most easily be obtained from the STF-CCF by setting $\delta_T = 0$ ($p = p'$), $\delta_R = 0$ ($q = q'$), and $\upsilon' = 0$, i.e., $r_{pq}(\tau) = r_{pq,pq}(0, 0, 0, \tau)$. Note that the temporal ACF $r_{pq}(\tau)$ is identical for all links $A^T_p - A^R_q$.

Finally, the FCF $r_{\tau'}(\upsilon')$, defined as $r_{\tau'}(\upsilon') := E\{H_{pq}(f', t)^* H_{pq}(f' + \upsilon', t)\}$, can be obtained from the STF-CCF by setting $\delta_T = 0$ ($p = p'$), $\delta_R = 0$ ($q = q'$), and $\tau = 0$, i.e., $r_{\tau'}(\upsilon') = r_{pq,pq}(0, 0, \upsilon', 0)$.

V. Numerical results

In this section, we illustrate the analytical results presented in the previous section. The following model parameters have been chosen. The carrier frequency f_c was equal to 2.45 GHz, corresponding to a wavelength of $\lambda = 122.45$ mm. The mobile speeds have been set to $\mathrm{v}_T = \mathrm{v}_R = 20$ km/h, and the directions of motion are $\phi_T = \pi/2$ and $\phi_R = -\pi$. The tilt angles of the antenna arrays are determined by $\gamma_T = 0$ and $\gamma_R = \pi/2$. The street parameters are chosen as $h^T_1 = h^T_2 = 10$ m and $h^R_1 = h^R_2 = 10$ m. For the mean powers of the single-bounce and double-bounce components, we have selected the values $\eta_{\mathrm{SBR}} = \eta_{\mathrm{SBT}} = \eta_{DB} = 1/3$. The AODs and AOAs are supposed to be uniformly distributed within their domains as they are specified in the appendix. Figure 3, illustrates the absolute value of the resulting spatial CCF $|\rho_{11,22}(\delta_T, \delta_R)|$. Impressions of the absolute values of the temporal ACF $|r_{pq}(\tau)|$ and the FCF $|r_{\tau'}(\upsilon')|$ can be gathered from the graphs in Figs. 4 and 5, respectively. These figures show the influence of D_x and D_y on the temporal and frequency correlation properties. As it can be observed from Fig. 4, the absolute value of the temporal ACF $|r_{pq}(\tau)|$ decays faster with decreasing parameters D_x and D_y. In fact, as the transmitter and the receiver approach the intersection point, the angular spread of the AOD and the AOA increase, which results in a faster decay of the temporal ACF around the origin. The opposite effect can be observed in Fig. 5. It is obvious that if D_x and D_y decrease, the delay spread and thus the coherence bandwidth decreases as well, which explains the slower decay of the FCF around the origin.

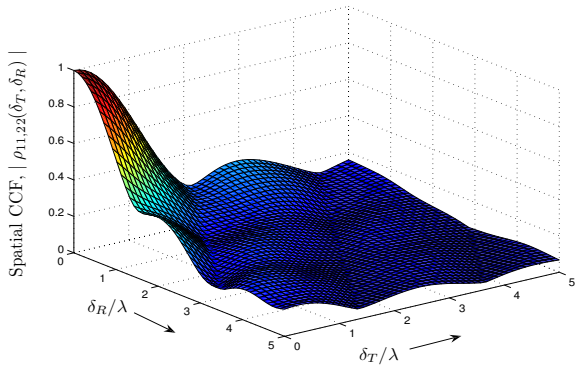

Fig. 3. Absolute value of the spatial CCF $|\rho_{11,22}(\delta_T, \delta_R)|$ of the T-model for $D_x = D_y = 15$ m.

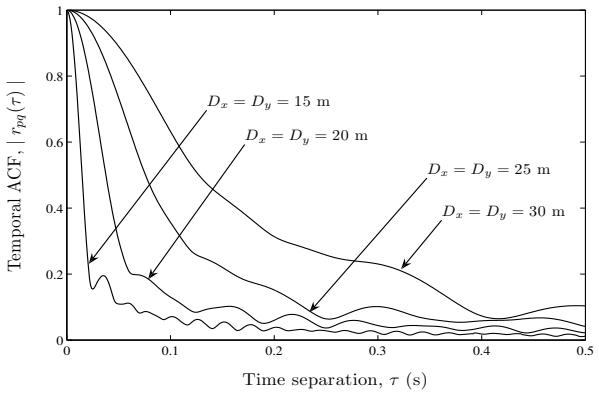

Fig. 4. Absolute value of the temporal ACF $|r_{pq}(\tau)|$ of the T-model.

VI. Conclusions

In this paper, we have presented a new MIMO V2V channel model for T-junction environments. The statistical properties of this so-called T-model have been studied with emphasis

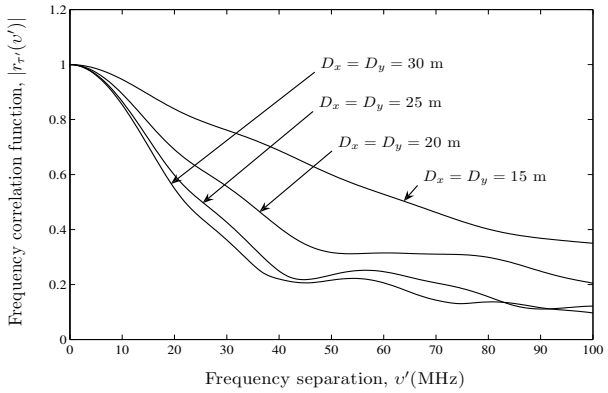

Fig. 5. Absolute value of the FCF $|r_{\tau'}(v')|$ of the T-model.

on the spatial, temporal, and frequency correlation functions. These correlation functions can be controlled by a variety of parameters making the T-model highly flexible. This model is therefore a proper candidate for capturing the propagation characteristics of a variety of V2V street channels in different propagation environments typical for T-intersections with corner buildings and/or other roadside obstructions. The study of the temporal ACF and the FCF has shown that as the transmitter and the receiver approach the intersection point, the channel coherence time decreases while the channel coherence bandwidth increases. Supported by our analysis, we believe that the proposed channel model is useful for the test, design, and analysis of inter-vehicle communication systems.

APPENDIX

In this appendix, we present the exact relationships between the AODs and AOAs of the T-model. The relationships can be determined by applying trigonometric identities on the geometric T-junction scattering model illustrated in Fig. 2. In case of single-bounce scattering, the final result for the relationship between the AOA β_m^T and the AOD α_m^T can be expressed as

$$\beta_m^T = \pi + \arctan\left(\frac{D_y + h_1^R + h_1^T \cdot \tan(\alpha_m^T)}{D_x + h_1^T + h_2^T}\right) \quad (29)$$

for $\alpha_m^T \in [\alpha_{\min}^T, \alpha_{\max}^T]$, where

$$\alpha_{\min}^T = \pi - \arctan\left(\frac{D_y + h_1^R}{h_1^T}\right) \quad (30)$$

$$\alpha_{\max}^T = \pi - \arctan\left(\frac{D_x \cdot D_y - h_1^R \cdot (h_1^T + h_2^T)}{D_x \cdot h_1^T}\right). \quad (31)$$

The AOA β_n^R can be expressed in terms of the AOD α_n^R as

$$\beta_n^R = \pi - \arctan\left(\frac{h_2^R \tan(\alpha_n^R)}{\tan(\alpha_n^R)(D_x + h_2^T) - (h_1^R + h_2^R + D_y)}\right) \quad (32)$$

for $\alpha_n^R \in [\alpha_{\min}^R, \alpha_{\max}^R]$, where

$$\alpha_{\min}^R = \arctan\left(\frac{D_y}{h_2^T}\right) \quad (33)$$

$$\alpha_{\max}^R = \arctan\left(\frac{D_y + h_1^R + h_2^R}{h_2^T}\right). \quad (34)$$

In the double-bounce case, the AOA β_n^R is independent of the AOD α_m^T. Note that the AOD α_m^T is within the range from $\alpha_{\min}^T$ [see (30)] to $\alpha_{\max}^T$ [see (31)], and the AOA β_n^R is confined to the interval $[\beta_{\min}^R, \beta_{\max}^R]$, where

$$\beta_{\min}^R = \pi - \arctan\left(\frac{D_y \cdot h_2^R}{D_x \cdot D_y - h_2^T \cdot (h_1^R + h_2^R)}\right) \quad (35)$$

$$\beta_{\max}^R = \pi - \arctan\left(\frac{h_2^R}{D_x}\right). \quad (36)$$

REFERENCES

[1] ASTM, "Standard specification for telecommunications and information exchange between roadside and vehicle systems - 5 GHz band dedicated short range communications (DSRC) medium access control (MAC) and physical layers (PHY) specifications," ASTM, Tech. Rep. ASTM E2213-03, Sept. 2006.

[2] M. Pätzold, B. O. Hogstad, and N. Youssef, "Modeling, analysis, and simulation of MIMO mobile-to-mobile fading channels," *IEEE Trans. Wireless Commun.*, vol. 7, no. 2, pp. 510–520, Feb. 2008.

[3] J. Maurer, T. Fügen, T. Schäfer, and W. Wiesbeck, "A new inter-vehicle communications (IVC) channel model," in *Proc. 60th IEEE Veh. Technol. Conf., VTC'04-Fall*, vol. 1. Los Angeles, CA, USA, Sept. 2004, pp. 9–13.

[4] A. Paier, J. Karedal, N. Czink, H. Hofstetter, C. Dumard, T. Zemen, F. Tufvesson, A. F. Molisch, and C. F. Mecklenbräucker, "Car-to-car radio channel measurements at 5 GHz: pathloss, power delay profile, and Doppler delay spectra," in *Proc. 4th IEEE International Symposium on Wireless Communication Systems, ISWCS 2007*. Trondheim, Norway, Oct. 2007, pp. 224–228.

[5] D.-S. Shiu, G. J. Foschini, M. J. Gans, and J. M. Kahn, "Fading correlation and its effect on the capacity of multielement antenna systems," *IEEE Trans. Commun.*, vol. 48, no. 3, pp. 502–513, Mar. 2000.

[6] M. Pätzold and B. O. Hogstad, "A space-time channel simulator for MIMO channels based on the geometrical one-ring scattering model," in *Proc. 60th IEEE Semiannual Veh. Technol. Conf., VTC 2004-Fall*, vol. 1. Los Angeles, CA, USA, Sept. 2004, pp. 144–149.

[7] C. S. Patel, G. L. Stüber, and T. G. Pratt, "Simulation of Rayleigh faded mobile-to-mobile communication channels," in *Proc. 58th IEEE Veh. Technol. Conf., VTC'03-Fall*. Orlando, FL, USA, Oct. 2003, pp. 163–167.

[8] M. Pätzold and B. O. Hogstad, "A wideband MIMO channel model derived from the geometrical elliptical scattering model," *Wireless Communications and Mobile Computing*, vol. 8, pp. 597–605, May 2008.

[9] A. Chelli and M. Pätzold, "A MIMO mobile-to-mobile channel model derived from a geometric street scattering model," in *Proc. 4th IEEE International Symposium on Wireless Communication Systems, ISWCS 2007*. Trondheim, Norway, Oct. 2007, pp. 792–797.

[10] A. F. Molisch, A. Kuchar, J. Laurila, K. Hugl, and E. Bonek, "Efficient implementation of a geometry-based directional model for mobile radio channels," in *Proc. 50th IEEE Veh. Technol. Conf., VTC'1999-Fall*. Amsterdam, Netherlands, Sept. 1999, pp. 1449–1453.

[11] C. Wei, H. Zhiyi, and Y. Tianren, "A street reference model of MIMO vehicle-to-vehicle fading channel," in *Proc. 3rd IEEE Conference on Industrial Electronics and Applications, ICIEA 2008*. Singapore, 2008, pp. 275–278.

[12] A. G. Zajić, G. L. Stüber, T. G. Pratt, and S. Nguyen, "Statistical modeling and experimental verification of wideband MIMO mobile-to-mobile channels in highway environments," in *Proc. 19th IEEE Int. Symp. on Personal, Indoor and Mobile Radio Communications, PIMRC 2008*. Cannes, France, Sept. 2008.